Chapter 17:

Helium Ion Microscope Fabrication of Solid-State Nanopore Devices for Biomolecule Analysis

Osama K. Zahid and Adam R. Hall

Virginia Tech-Wake Forest School of Biomedical Engineering and Sciences, Wake Forest University

School of Medicine, Winston Salem, NC 27101, USA

Abstract: Solid-state nanopores are an emerging technology for the detection and analysis of biomolecules at the single-molecule level. Consisting of one or more nanometer-scale apertures in a thin, solid-state membrane, a number of methods have been utilized to make these devices. However, conventional approaches are either non-trivial to scale up or lack sufficient precision for many applications. In this chapter, we describe the use of the helium ion microscope to produce nanopores. We demonstrate control over diverse aspects of the device and discuss a range of applications that have been enabled by their implementation.

1. Introduction

In the 1940s, Wallace H. Coulter developed a method of quantifying blood cells[1] that was initially criticized for being unsophisticated. The apparatus was built by producing a hole of ~10 µM in a cellophane cigarette wrapper and placing it in between two isolated chambers containing electrolyte solution, thus ensuring the opening as the only passage through which the chambers could interact. The application of an electrical bias between the two chambers generated a measurable ionic current that corresponded linearly to the applied voltage and when cells in solution were forced through the pore by pressure, their brief presence resulted in a transient decrease in the ionic current. The number of spikes, or resistive pulses, could be used to enumerate the cells while their individual amplitudes were shown to correspond to cell type (red or white blood cell), since these differ in volume and displace ions proportionally. This simple detection principle is at the core of the Coulter

Counter technology that has revolutionized the field of hematology and is still widely employed in the clinic [2].

Several decades later, another revolution is underway that is based on the same principle, but instead occurs at the nanoscale and probes individual molecules. This is being realized by the emerging technology of solid-state (SS-) nanopores[3, 4], wherein a nanometer size aperture is generated in an insulating membrane, most commonly through the use of charged particle beam fabrication techniques. As in the Coulter device, the chip containing a nanopore is positioned in a flow cell and electrolyte solution is introduced to the chambers, enabling a voltage-induced ionic current that can be measured in real-time using a patch-clamp amplifier. Using this system, molecules like DNA[5, 6], RNA[7], proteins[8, 9], and nanoparticles[10, 11] can be electrically threaded from one side (*cis* chamber) to the other (*trans* chamber) while being individually probed (Fig. 1).

Investigation at the molecular scale using SS-nanopores was first demonstrated[12] by the Golovchenko group in 2001 and has since been developed into a remarkably expansive technology, extending far beyond simple counting. For example, the system has been used to probe DNA-protein interactions[13–16], DNA epigenetics[17–19], and nucleic acid biomarkers[20, 21], and used to generate devices that mimic nanopores found in nature, like the nuclear pore complex[22] and porins[23]. Simultaneously, significant advancements have been made towards understanding the fundamental physics of nanoscale confinement, such as ionic screening[24], electrical forces[25–27], translocation dynamics[6, 28], and the effects of solvent conditions[29–34]. Understanding these mechanisms is important both for improving devices and for developing novel measurement techniques.

Critical to all of these areas has been the realization of the SS-nanopore devices themselves, towards which several fabrication methods have been developed. The first demonstrated approach was ion beam sculpting[12], in which a defocused ion beam is used to controllably reduce the size of a pre-fabricated micropore. By monitoring ionic flux during the closing, a single nanopore can be produced with sub-nanometer precision. Soon after, devices were also demonstrated using

transmission electron microscope (TEM) ablation of a thin membrane[35]. Similar precision is achievable with this method, and by virtue of the relative availability of TEM systems, it has become widely embraced by the field. Later, Ga+ focused ion beam (FIB) milling was also shown to be able to produce nanopores[36]. However, each of these charged particle beam approaches has significant challenges. For instance, both ion beam sculpting and TEM are low-throughput techniques, able to accommodate only a single device at a time, and can require many minutes to hours to produce a single pore. Ga+ FIB overcomes throughput, but at the expense of precision and resolution; it can typically produce pores only as small as about 15 nm and with low reproducibility. More recent innovations like the dielectric breakdown technique[37] offer tremendous advantages in fabrication cost, but may still have limitations in aspects of fabrication like throughput or array formation.

One candidate technology that can address many of these challenges is the scanning helium ion microscope (HIM). In this chapter, we review HIM nanofabrication as it relates to SS-nanopores, showing not only rapid and precise pore definition, but also the ability to manipulate other device properties as well. Finally, we describe a wide range of biosensing applications that have been and are currently being addressed using HIM SS-nanopores.

2. HIM Milling of SS-nanopores

Milling by FIB is a well-characterized process that occurs by sputtering[38] when ions impinge on a surface with sufficient acceleration to knock out substrate atoms through nuclear-nuclear interactions (Fig 2 scheme). The minimum feature resolution achievable through sputtering depends principally on two factors: the amount of momentum transfer and the size of the focal spot (i.e. exposure area). For example, conventional FIB uses large Ga+ ions (70 amu) with a typical acceleration voltage of 5-30 kV and can achieve a focal spot[39] of only ~10 nm. Consequently, the smallest nanopores that can be realized by the approach are ~10-20 nm, with low reproducibility[36, 40]. By virtue of using much smaller He+ ions (4 amu), an atomically sharp source, and advanced

focusing optics to achieve a focal spot[41] of ~0.34 nm, HIM improves significantly on these resolution limitations. As a result, it is a superior technology for the fabrication of SS-nanopores.

2.1 Nanopore Formation

Nanopores were fabricated in a thin, free-standing silicon nitride (SiN) membrane supported by a Si chip. For the measurements presented here, we used 30 nm thick SiN membranes that span an area of ~250 μm^2 in a 4.4 mm Si support frame with a thickness of 200 μm. Considering this particular size and the 50 mm X-Y travel range of the HIM sample stage, up to a 100 individual devices could be processed in a single sample exchange load cycle. However, the process is amenable to a wide range of device dimensions that could enable even more. Before mounting, chips are rinsed with acetone and ethanol, dried under nitrogen gas flow, and subsequently placed in a custom-built HIM sample holder. The holder containing the samples was treated under oxygen plasma (150 W) for 2-5 minutes to ensure removal of organic contaminants and was then immediately placed in the HIM sample exchange chamber, where it underwent a further 3 minutes of air plasma treatment (10 W) before being transferred into the main chamber. This ensured elimination of minor contamination acquired in transit.

Once the sample stage was transferred into main imaging chamber, HIM beam current was adjusted through selection of appropriate condenser lens setting and aperture size and adjustment of He supply pressure. We typically utilized currents of at least 5 pA for SS-nanopore fabrication, but have achieved good results with at <1 pA as well. Low magnification imaging of the Si chip was used to determine the exact position of the SiN window and the beam was positioned on the Si substrate immediately adjacent to it. To ensure that the beam focus and stigmation was fine-tuned prior to fabrication, a brief (5-10 sec) single spot exposure of the beam was used to produce a feature in the substrate that was subsequently used to optimize the beam conditions in conventional imaging mode. Immediately following this, the beam was blanked and the SiN window was moved into the beam path. Lithographic control elements were then used to perform beam exposure for a set time,

progressively sputtering material and generating a single nanopore. Using measurements from low-energy (<150 kV) TEM images, we have found that SS-nanopore size varies with total incident ion dose (Fig. 2b). For a given dose, we observed only minor variation (±2-3 nm) in pore diameter, indicating high reproducibility. Post-fabrication analysis of the pore can also be acquired through transmission imaging, but resolution is limited and the imaging beam may affect pore dimensions.

The ionic resistance of each pore can also be used to confirm the fabricated dimensions using a simplified conductance model. Toward this end, a chip containing a single SS-nanopore was rinsed with clean deionized water (DiH$_2$O) and pure ethanol and then dried under air flow. Following an air (or oxygen) plasma treatment (15 W) for 2-5 mins per side, the chip was positioned in a custom flow cell and high ionic strength electrolyte solution (1 M KCl) was introduced to both sides of the device. Ionic current was measured with a commercial patch-clamp amplifier (Axopatch 200B, Molecular Devices) by way of a pair of Ag/AgCl electrodes. All devices exhibited linear I-V curve characteristics and steady, low noise baseline current. Indeed, comparison of identical devices fabricated by TEM and HIM showed no significant difference in noise characteristics[42]. The diameter, d, of a SS-nanopore can be determined from its measured conductance, G, through the equation[29]

$$G = \frac{\pi d^2}{4L_{eff}}\left((\mu_K + \mu_{Cl})n_K e + \frac{4\sigma\mu_K}{d}\right),$$

where L_{eff} is the effective thickness of the membrane near the nanopore, μ_K and μ_{Cl} are the electrophoretic mobilities of potassium and chloride (7.616 and 7.909 × 10^{-8} m^2 V^{-1} s^{-1}, respectively), n_K is the number density of counterions, e is the elementary charge and σ is the surface charge density of the membrane material. This model provides an independent verification of device dimensions, which we find to be in good agreement with direct TEM analysis[42].

In general, ion milling can be described by the relation[43]:

$$\log(d) = a + b\log(D),$$

where d is feature dimension (SS-nanopore diameter), a and b are correlation constants, and D is the total ion dose. As a result, HIM pore formation would be expected to manifest as a linear relationship

on a log-log scale. However, we clearly observe two separate linear regimes: a fast pore growth rate regime below for small diameters, which then transitions to a slower increase for larger diameters[42]. This transition occurs consistently at a diameter of ~10 nm across a range of initial conditions[44]. We interpret this observation to be the result of nanopore shape. The intense center of the Gaussian beam is able to sputter the initial SiN membrane efficiently, resulting in a high growth rate. However, beyond the Full Width Half Maximum (FWHM), sputtering is induced only by the less intense edges of the beam, resulting in a significantly lower yield. Thus the transition between these two regimes is related to beam characteristics and is intrinsic to the approach.

2.2 DNA Translocation

Having established the ability to produce SS-nanopores with HIM milling, we next turn to the central aspect of their utility in single-molecule detection. While ionic current measurements were demonstrated, a number of factors could be important to supporting molecular translocation, including implanted charge, surface roughness, and microscopic pore shape. Therefore, direct confirmation of device viability is critical.

We used translocation of the well-characterized λ bacteriophage double-stranded (ds-) DNA genome (48 kbp) as a model because it is the most widely studied material in the field and is therefore an ideal benchmark. Figure 3a shows a typical conductance trace with characteristic discrete event amplitudes at integer multiples of the first non-baseline conductance level. The spacing of these event profiles (Fig. 3b) are indicative of the conformation of DNA molecules as they pass through the pore: a molecule translocating linearly reduces the conductance by a standard amount; a singly-folded molecule reduces it twice as much, and so on (Fig. 3c). These data are in agreement with numerous previous reports[5, 6] and confirm that translocations dynamics through HIM nanopores are essentially indistinguishable from those made by other fabrication methods.

2.4 Nanopore arrays

SS-nanopore arrays will enable parallel sensing platforms that have high throughput and thus potential for wide-ranging applications. While several studies have utilized nanopore arrays, the methods used to achieve them have suffered from either prolonged, manual fabrication time[22] or have required sophisticated post-fabrication treatments such as atomic layer deposition (ALD) to reduce pore sizes to optimal dimensions[45]. Each of these factors affects throughput and overall cost of production.

With HIM milling, arrays of arbitrary dimension and consisting of individual pores as small as 2-3 nm can be achieved. Using the integrated HIM lithographic system, the position and exposure time of each pixel in a pattern file can be controlled with no loss in resolution and no further alignment necessary. For example, Figure 2c shows an array of 100 individual SS-nanopores in a single device, each with a diameter of 5 nm. The total fabrication time for this array was about a minute. While the total number of pores can in principle be expanded without restraint, there are practical limits imposed by factors like sample linearity (substrate position relative to focal plane) and dynamic instrumental drift (stage, stigmators), which can alter beam conditions over time. Nonetheless, we have produced arrays of up to 10^4 pores and observed good reproducibility between the first and last pore formed.

2.5 Applications of HIM drilled Nanopores

SS-Nanopores offer the distinct advantage of single-molecule analysis of biomolecules and offers insight into their functions and interactions. Of the many potential and realized[46] applications of the platform, we describe here three research areas that have been impacted directly by HIM nanopores: induced DNA damage; nucleoprotein interactions; and selective quantification of DNA with single-base modifications.

DNA damage by depurination is a common process that occurs spontaneously under physiological conditions[47]. Here, the loss of adenine and guanine nucleotides occurs due to hydrolysis of the N-glycosyl linkages to the deoxyribose backbone resulting in an apurinic (AP) site. Under normal conditions, these lesions are repaired by the base excision pathway (BER) and

therefore occur at a low frequency. However evidence suggests in disease states such as cancers[48] and anemia[49] where homeostatic conditions are compromised, AP site damage is enhanced. Therefore, a rapid and direct determination of DNA damage would allow disease initiation and progression to be monitored. HIM nanopores have been employed to detect depurination using short (61bp) dsDNA molecules as a demonstration vehicle[50]. DNA depurination was induced by incubating molecules at various pH (ranging from 2-10) and subsequently performing SS-nanopore analysis. Under all investigated pH conditions, translocation event depth (amplitude) was found to be consistent, indicating conformational integrity. However, under increasingly acidic conditions, event durations transitioned from a single, defined population to a biomodal distribution (Fig. 4a). The first, unyielding population was attributed to translocation of unmodified dsDNA, while the second population emerged due to increased DNA damage. The generation of AP sites resulted in strand separations and unstructured regions that caused increased interaction with the pore walls. Excessively damaged DNA was shown to exhibit mean translocation durations more than an order of magnitude greater than the unmodified duration. Thus, the results clearly demonstrated label-free SS-nanopore detection and rough estimation of DNA depurination.

HIM nanopores have also been to used to analyze nucleoprotein structure. To this end, the selective interaction of single-stranded DNA binding protein (SSB) with single-strand (ss-) DNA to form nucleoprotein complexes was investigated[51]. Saturated nucleoprotein complexes were discriminated from free SSB, ssDNA and dsDNA individually by virtue of their characteristic translocation event depth (ΔG). Binding dynamics were also studied by titrating SSB against ssDNA. Figure 4b depicts ΔG histograms for SS-nanopore measurements as protein concentration was increased, showing that mean event depth shifts progressively due to complex formation. Additionally, nucleoprotein structure was probed by comparing linearized and circular ssDNA constructs, yielding a new model of filament formation.

As a final example, HIM SS-nanopores have been used to achieve selective detection and quantification of dsDNA featuring a single base modification[52]. This was realized through a novel

assay called drag-regulated nanopore translocation (DRNT). There are several key forces at play in the SS-nanopore system, including the driving force of electrophoresis (EP), the opposing force of electroosmosis (EO), and viscous drag. The net force experienced by a molecule determines its speed and direction, and consequently whether it can be detected by a SS-nanopore. For example, Plesa et al. demonstrated that most proteins are undetectable using conventional electronics due to rapid translocation speed[9]. Likewise, under conditions where EO force is comparable to or greater than EP, the translocation process is inhibited[24]. In DRNT, two types of undetectable molecule – one that threads rapidly and one that resists translocation – are transitioned to a resolvable speed via specific binding. In the initial demonstration, these components were a monovalent streptavidin (MS) [53, 54] protein variant that is compact and highly charged and thus experiences dominant EP force, and a short, dsDNA featuring a biotin tag (i.e. the high-affinity recognition molecule of streptavidin), which itself translocates at an insignificant rate under select conditions. However, when the components are bound together to form MS-dsDNA complex, a remarkable increase in the rate of translocation events is observed (Fig. 4c). This is a result of a rebalancing of forces such that the complex is pulled through the pore at a detectable speed. Since events were due exclusively to the bound population, event rate could be used to discriminate MS-dsDNA among a background. Indeed, biotinylated dsDNA was detected and quantified among a mixture of unlabeled molecules[52]. This powerful approach should be able to probe a wide range of biomolecules with intrinsic selectivity and sensitivity.

3. Manipulation of Device Thickness

The detection of small molecules or features along the length of large molecules is a specific challenge for SS-nanopore detection, driven largely by limitations in the signal-to-noise ratio (SNR) of the electrical measurement. One approach to addressing this challenge has been the use of nanopore devices fabricated in ultrathin membranes[20]. Toward this end, 2D materials such as graphene[56, 57], MoS_2[57], and boron nitride[58] are being pursued as alternate membrane

materials. However, integrating these materials is considerably more difficult than with Si-based materials, and they often bring with them additional challenges like substantial interaction with target biomolecules that can frustrate nanopore analysis[55]. An alternative approach instead aims to manipulate the thickness of conventional membranes through top-down processing. For instance, lithographically-defined reactive ion etching has been used to reduce the thickness of SiN membranes prior to SS-nanopore definition, thereby enabling analysis of short nucleic acids [20, 59] and protein structure[60]. However, this approach still requires considerable processing in addition to pore formation. HIM offers an ideal solution as a single method that is capable of both local manipulation of membrane thickness and nanopore milling.

3.1 Membrane thinning

Just as sufficient HIM beam dose at a single point can result in complete sputtering of SiN atoms to form nanopores, exposure to a reduced dose across a localized region can induce more limited damage that can be used to control substrate thickness. In the case of a thin membrane, there are two types of sputtering interactions to consider: direct sputtering, which occurs by removal of atoms by direct interaction at the point of incidence, and transmission sputtering, which occurs by both direct and indirect removal of atoms at the opposite (exiting) surface (Fig 5a). Both of these contribute to membrane manipulation and must be characterized to achieve a desired thickness.

Early investigation[61] of this process focused on direct topographic analysis by atomic force microscopy (AFM). To accomplish this, two Si chips containing SiN membranes were introduced to the HIM chamber, one with its flat (unetched) surface facing up and one facing down, and the beam condition was adjusted as described in Section 2. Here, an initial membrane thickness of 105 nm was used for easier characterization. HIM lithographic patterning was then used to produce an identical series of 500 nm square patterns on each chip with increasing total doses. Importantly, each pattern was exposed by repeatedly rastering over the pattern to reduce redeposition of ablated material[62] or sample charging. Following processing, the flat surface of each chip was analyzed by AFM for a

complete quantitative description. From these measurements, direct milling depth was found to vary linearly with total incident ion dose while transmission milling depth varied with the square of the dose. While transmission milling was considerably less efficient than direct milling, as expected qualitatively from its mechanistic nature, it was found to contribute significantly to overall membrane thickness. Thus, the combination of these two milling rates could enable arbitrary membrane thickness to be achieved.

While robust, the AFM approach adds additional analytical burden to the membrane thinning process. A more powerful technique was realized when scanning transmission ion microscopy (STIM) was shown to allow quantitative, *in situ* assessment of membrane thickness[63]. In STIM, an image is formed using secondary electrons produced at a metal surface below the SiN membrane. In this case, image brightness is reduced by scattering losses in the beam, and so thinned regions will appear progressively brighter than the surrounding membrane (Fig. 5b). Crucially, pixel brightness was demonstrated to scale directly with membrane thickness, such that a single calibration of image brightness to actual membrane dimension (Fig. 5c) enables thickness determination from a single STIM image. As a result, membrane manipulation and characterization could be achieved in a single step.

3.2 HIM control of SS-nanopore device dimensions

Subsequent to membrane thinning, SS-nanopores can be fabricated in the in the same processing step (Figure 6a). However, the dose-diameter relationship of HIM pore formation (see Section 2.1) depends acutely on membrane characteristics. As a result, a quantitative understanding how pore formation varies with membrane thickness is critical.

An assessment of this interplay was carried out by measuring SS-nanopore diameter dependence on exposure dose as a function of membrane thickness[44]. Because thinner membranes require less sputtering to produce a pore of a given size, the trend is observed to shift to lower dose with a monoexponential dependence as membrane thickness is reduced (Fig. 6b). This

analysis enables comprehensive control over SS-nanopore device dimensions in a single step. Using these findings, pores as small as 2 nm can be produced in a membrane only 1.4 nm thick (Fig. 6b inset). It is also important to note that regardless of the membrane thickness, pore formation follows the same two-regime growth that was observed in native membranes[42], with the transition from fast to slow growth appearing consistently at a ~10 nm diameter.

To confirm the viability of HIM-thinned devices and their utility in enhancing SNR, a comparative analysis of dsDNA translocations through SS-nanopores with identical diameters (~3.2 nm) fabricated in membranes with disparate thickness (4.5 ± 0.6 nm and 24.5 ± 0.8 nm, respectively) was conducted. Ionic current was used to confirm the device dimensions before measurement, showing that actual pore diameter matched well with the target size. Measurement of 3 kbp dsDNA translocation events showed conclusively[44] that use of the thinned device improved SNR by about a factor of 2 (Fig 6c).

3.3 Applications of HIM-thinned SS-nanopores

While the operating principle of resistive pulse sensing is straightforward, the resulting electrical signals can be surprisingly complex and thus challenging to interpret. One source of this behavior is the interaction of biomolecules with the access regions[64], a sensing volume that extends from both openings of the nanopore and into the measurement solution. Several studies have suggested that complicated conductance blockade levels can arise for dsDNA due to stochastic interactions with the access regions or occur prior to threading of dsDNA into the pore[7, 65–68]. However, a definitive explanation has not been presented, in part due to SNR limitations in conventional devices. SS-nanopores formed in HIM-thinned SiN membranes have enabled new investigations into the origin of these heretofore unexplained aspects of translocation events[69]. Figure 7 shows an example of signal complexity, depicting event depth (ΔG) histograms with Gaussian fits (grey lines) for 3 kbp dsDNA translocations through a 3.4 nm diameter pore fabricated in a 4.5 nm thick membrane. Crucially, across all investigated voltages (50-400mV), distinct populations emerged, the mean ΔG of

which evolve with applied voltage (Fig 7a). Each conductance population was attributable to a distinct type of interaction: the deepest events (green) were caused by non-translocative perpendicular blockages of the pore by the dsDNA; the intermediate level events (blue) were linear translocation through the pore; and shallow events (red) were transient interactions with only the access region (Fig. 7b). Each of these could be described by a simple geometric model. A detailed understanding of translocation dynamics and elucidation of translocation signals is important towards accurate data assessment and analysis in all SS-nanopore measurements, but especially in studies using thin nanopore devices[19, 70] where these effects are pronounced.

4. Manipulating Intrinsic Membrane Fluorescence

The conventional measurement of conductance through SS-nanopores has been a powerful tool for biomolecule characterization, but has limitations. Critically, electrical measurements on multiple nanopores simultaneously is challenging, requiring sophisticated electronics and separated measurement chambers. As a result, massively parallel detection schemes are difficult to execute, in spite of the potential benefit to detection throughput and costs. An alternate approach that could address this obstacle is the employment of single-molecule fluorescence as the detection mechanism. Here, the use of fluorescent molecules or buffer components[71–73] allows translocations to be monitored through direct, high-speed optical during the application of voltage. The technique offers several potential advantages. First, direct observation can be conducted in wide-field, enabling simultaneous detection on arbitrary numbers of pores, limited only by field of view and diffraction. Furthermore, the use of multispectral imaging and the integration of powerful techniques like total internal reflection microscopy (TIRF)[74] and Förster resonance energy transfer (FRET)[75] could facilitate additional flexibility, sensitivity, and selectivity.

A critical factor in optical detection is the photoluminescence (PL) of the solid-state membrane. Intrinsic PL increases the fluorescence noise floor, and so should be minimized in an ideal device to maximize resolution and to enable a wide-array of flourophores. Importantly, most common

membrane materials exhibit considerable PL, including SiN, which emits in the important wavelength range of 400-800 nm. However, few studies have addressed PL in optical SS-nanopore detection. Recently, dela Torre *et al.* demonstrated[45] that atomic layer deposition of TiO_2 could be used on nanopores fabricated in SiN by FIB to both control pore diameter and reduce membrane PL. Additionally, Schmidt *et al.*[76] used electrochemical etching to fabricate nanopore arrays in a silicon membrane, chosen in part for its low inherent PL. However, these methodologies required additional fabrication steps or produced thick devices with low yield, respectively. Therefore, there is a need for integrated fabrication techniques that can rapidly address membrane PL and produce SS-nanopores concomitantly.

4.1 HIM Photoluminescence Reduction

SiN PL is thought to arise from the presence of nanocrystalline domains within the matrix that act as radiative centers[77, 78]. Therefore, amorphization of those domains is a direct route to controllable reduction of membrane PL. With HIM, it has been demonstrated[79] that the beam penetrates substrate material efficiently, resulting in atom-atom interactions and implantations that can affect the internal structure. Therefore, by utilizing beam doses lower than the SiN surface binding energies (i.e. doses that do not sputter significant material), internal amorphization could be achieved with minimal change to membrane thickness or roughness (Fig. 8a).

To investigate this, a 30 nm thick SiN membrane was patterned with varying He+ ion doses, similar in methodology to membrane thinning described above (Section 3.1), and then imaged using TIRF microscopy. This treatment resulted in a clear reduction of membrane PL (Fig. 8b) that decreased exponentially with ion exposure. For example, greater than 90% of membrane PL was removed with a dose of 300-400 ions/nm^2; an exposure that would result in a mean decrease in membrane thickness of less than 1 nm. As a result, removal of essentially all PL does not significantly alter overall membrane morphology.

Following PL suppression, the HIM beam can subsequently be used to fabricate SS-nanopores within the patterned region using the dose-diameter relationship of the native membrane. The device can then be used to detect fluorescently-labeled biomolecules with minimal interference. As a demonstration, a 4 μm square region was exposed with a dose of 400 ions/nm^2 to remove PL and a single 5 nm pore was subsequently fabricated at its center. After mounting the device in a custom holder, a 2.8 kbp dsDNA with a fluorophore label (Cy3) was introduced and subjected to electrokinetic translocation. Figure 8c shows typical traces obtained from the device, first in the form of conventional ionic current measurement and then as dynamic nanopore fluorescence derived from high-speed video (500 Hz) of TIRF observation during the applied voltage. While these measurements could not be conducted simultaneously, analysis of both traces yielded event rates 0.45 Hz, demonstrating correlative results.

4.2 Application of HIM Photoluminescence Reduction

Optical detection can enable massively parallel detection schemes by allowing analysis of dynamic fluorescence across many SS-nanopores simultaneous. An important design aspect to consider for this purpose is the ability to accurately localize each individual pore. The HIM fabrication process addresses this issue inherently. Since the total He+ ion beam diameter (i.e. the full width of its Guassian intensity profile) is larger than the nanopore that results from a single point exposure, the region around the pore edges is subjected a significant ion dose that decreases radially in intensity. The local PL is thus suppressed during normal pore formation, manifesting as a non-emitting region around the pore that can typically extend 100-300 nm past the edge of the SS-nanopore[79].

In following, the PL of a 5 um square region in a SiN membrane was reduced by ~80%, and an array of 400 individual SS-nanopores (diameter ~5 nm) was fabricated in its confines. Each individual pore is resolvable as a dark spot in a wide-field TIRF micrograph (Fig. 9a). DNA translocations were then performed under application of 1 V bias and while collecting TIRF microscopy images at a rate of 675 Hz. To avoid issues with pore-fouling, short (55 nt) ssDNA homopolymers were investigated,

each containing 3 Cy3 fluorophores. Stochastic increases in fluorescence intensity could be observed at the site of individual SS-nanopores (Fig. 9b), indicative of molecular translocations; importantly, such analysis could be performed simultaneously across the array with a single video.

Transient diffusion of labeled molecules into the sensing volume could contribute to the optical translocation events observed in these traces. To explore this issue, dynamic fluorescence intensity was also analyzed in regions adjacent to the array, but not at the location of a pore, where diffusion can still deliver molecules but there is no electrical driving force. The rate of events in these regions was found to be 0.03 Hz; about an order of magnitude lower than the 0.27 Hz rate observed at the location of SS-nanopores. Therefore, at least 90% of the optical events collected throughout the nanopore array are attributable to electrokinetic translocation.

5. Conclusions and Outlook

In conclusion, HIM milling is a versatile and rapid technique for fabricating SS-nanopores devices, offering tremendous control over device dimensions and properties. The capabilities of this approach are best captured as a function of He+ ion dose (Fig. 10). At high doses ($>\sim 10^6$ ions/nm^2), the HIM beam can rapidly sputter membrane material to form SS-nanopores. Through control of beam current and exposure time, pore diameters can be produced with high precision ($\pm$2-3 nm) and resolution (down to ~2.5 nm). Crucially, HIM features like a large range of stage motion and lithographic beam control enable high throughput processing and array formation as well. At intermediate doses ($\sim 10^3$-10^5 ions/nm^2), the HIM beam is able to sputter some but not all membrane material, resulting in controllable reduction in thickness. This process is patternable and can be used to realize membrane regions as thin as 1-2 nm, which can subsequently be targeted for SS-nanopore formation to achieve high measurement sensitivity. Finally, at low doses ($<\sim 10^3$ ions/nm^2), the HIM beam can be used to control intrinsic membrane PL by causing internal structural deformation (e.g. amorphization of radiative centers) without inducing significant sputtering. As a result, membrane fluorescence can be reduced or removed while maintaining its initial dimensions. Subsequently, PL reduction was

achieved using TEM as well[80], however that instrument is difficult to incorporate into high-throughput fabrication.

We have described here several applications of HIM SS-nanopore devices that take advantage of the various aspects enabled by the fabrication method. From selective detection of modified DNA to elucidating electrokinetic translocation dynamics to massively parallel sensing, these efforts establish the utility of both the platform in general and devices produced by HIM in particular. In continuing work, these measurements will be expanded and improved. For example, the DRNT assay developed with HIM nanopores is currently the focus of extensive research as a possible route toward nucleic acid biomarker identification. Such a capability could be a valuable asset for the rapid diagnosis of diseases like cancer[81] and Alzheimer's disease [82]. Additionally, the potential for massively-parallel analysis could be an important capability for a future high-throughput genetic sequencing device[83].

SS-nanopores hold remarkable potential as the basis of a wide range of cost-effective and highly sensitive detection devices. As a consequence, they could revolutionize the future of medical diagnostics, just like the Coulter Counter did decades ago. However, one of the most daunting obstacles to their development and integration is simple availability. Since the introduction of platform, several fabrication strategies have been effectively employed, but each has brought with it significant limitations in speed, resolution, or throughput. As we have discussed here, HIM addresses each of these challenges while also offering tremendous flexibility in controlling a range of additional device characteristics that will result in a more versatile system. Accordingly, the capabilities afforded by helium ion microscopy will play a critical role in the future of SS-nanopore technologies.

References

[1]   W. H. Coulter, "Means for Counting Particles Suspended in a Fluid," US2656508 A, Oct 20, 1953.

[2]   M. D. Graham, "The Coulter Principle: Foundation of an Industry," *J. Assoc. Lab. Autom.*, vol. 8, no. 6, pp. 72–81, 2003.

[3]   C. Dekker, "Solid-State Nanopores," *Nat. Nanotechnol.*, vol. 2, no. 4, pp. 209–215, Apr. 2007.

[4]   M. Wanunu, "Nanopores: A Journey towards DNA Sequencing," *Phys. Life Rev.*, vol. 9, no. 2, pp. 125–158, 2012.

[5]   J. Li, M. Gershow, D. Stein, E. Brandin, and J. A. Golovchenko, "DNA Molecules and Configurations in a Solid-State Nanopore Microscope," *Nat. Mater.*, vol. 2, no. 9, pp. 611–5, 2003.

[6]   A. J. Storm, C. Storm, J. Chen, H. Zandbergen, J.-F. Joanny, and C. Dekker, "Fast DNA Translocation through a Solid-State Nanopore," *Nano Lett.*, vol. 5, no. 7, pp. 1193–1197, 2005.

[7]   G. M. Skinner, M. van den Hout, O. Broekmans, C. Dekker, and N. H. Dekker, "Distinguishing Single- and Double-Stranded Nucleic Acid Molecules using Solid-State Nanopores," *Nano Lett.*, vol. 9, no. 8, pp. 2953–2960, 2009.

[8]   D. Fologea, B. Ledden, D. S. McNabb, and J. Li, "Electrical Characterization of Protein Molecules by a Solid-State Nanopore," *Appl. Phys. Lett.*, vol. 91, no. 5, p. 053901, 2007.

[9]   C. Plesa, S. W. Kowalczyk, R. Zinsmeester, A. Y. Grosberg, Y. Rabin, and C. Dekker, "Fast Translocation of Proteins through Solid-State Nanopores," *Nano Lett.*, vol. 13, no. 2, pp. 658–663, 2013.

[10]   A. R. Hall, J. M. Keegstra, M. C. Duch, M. C. Hersam, and C. Dekker, "Translocation of Single-Wall Carbon Nanotubes through Solid-State Nanopores," *Nano Lett.*, vol. 11, no. 6, pp. 2446–2450, 2011.

[11] K. E. Venta, M. B. Zanjani, X. Ye, G. Danda, C. B. Murray, J. R. Lukes, and M. Drndić, "Gold Nanorod Translocations and Charge Measurement through Solid-State Nanopores," *Nano Lett.*, vol. 14, no. 9, pp. 5358–5364, 2014.

[12] J. Li, D. Stein, C. McMullan, D. Branton, M. J. Aziz, and J. A. Golovchenko, "Ion-beam Sculpting at Nanometre Length Scales," *Nature*, vol. 412, no. 6843, pp. 166–169, 2001.

[13] G. V. Soni and C. Dekker, "Detection of Nucleosomal Substructures using Solid-State Nanopores," *Nano Lett.*, vol. 12, no. 6, pp. 3180–3186, 2012.

[14] D. Japrung, A. Bahrami, A. Nadzeyka, L. Peto, S. Bauerdick, J. B. Edel, and T. Albrecht, "SSB Binding to Single-Stranded DNA Probed Using Solid-State Nanopore Sensors," *J. Phys. Chem. B*, vol. 118, no. 40, pp. 11605–11612, 2014.

[15] R. M. M. Smeets, S. W. Kowalczyk, A. R. Hall, N. H. Dekker, and C. Dekker, "Translocation of RecA-Coated Double-Stranded DNA through Solid-State Nanopores," *Nano Lett.*, vol. 9, no. 9, pp. 3089–3095, 2009.

[16] S. W. Kowalczyk, A. R. Hall, and C. Dekker, "Detection of Local Protein Structures along DNA Using Solid-State Nanopores," *Nano Lett.*, vol. 10, no. 1, pp. 324–328, 2010.

[17] M. Wanunu, D. Cohen-Karni, R. R. Johnson, L. Fields, J. Benner, N. Peterman, Y. Zheng, M. L. Klein, and M. Drndić, "Discrimination of Methylcytosine from Hydroxymethylcytosine in DNA Molecules," *J. Am. Chem. Soc.*, vol. 133, no. 3, pp. 486–492, 2011.

[18] J. Shim, G. I. Humphreys, B. M. Venkatesan, J. M. Munz, X. Zou, C. Sathe, K. Schulten, F. Kosari, A. M. Nardulli, G. Vasmatzis, and R. Bashir, "Detection and Quantification of Methylation in DNA using Solid-State Nanopores," *Sci. Rep.*, vol. 3, 2013.

[19] J. Shim, Y. Kim, G. I. Humphreys, A. M. Nardulli, F. Kosari, G. Vasmatzis, W. R. Taylor, D. A. Ahlquist, S. Myong, and R. Bashir, "Nanopore-Based Assay for Detection of Methylation in Double-Stranded DNA Fragments," *ACS Nano*, vol. 9, no. 1, pp. 290–300, 2015.

[20]   M. Wanunu, T. Dadosh, V. Ray, J. Jin, L. McReynolds, and M. Drndić, "Rapid Electronic Detection of Probe-Specific MicroRNAs using Thin Nanopore Sensors," *Nat. Nanotechnol.*, vol. 5, no. 11, pp. 807–814, 2010.

[21]   A. Singer, S. Rapireddy, D. H. Ly, and A. Meller, "Electronic Barcoding of a Viral Gene at the Single-Molecule Level," *Nano Lett.*, vol. 12, no. 3, pp. 1722–1728, 2012.

[22]   S. W. Kowalczyk, L. Kapinos, T. R. Blosser, T. Magalhães, P. van Nies, R. Y. H. Lim, and C. Dekker, "Single-Molecule Transport Across an Individual Biomimetic Nuclear Pore Complex," *Nat. Nanotechnol.*, vol. 6, no. 7, pp. 433–438, 2011.

[23]   A. R. Hall, A. Scott, D. Rotem, K. K. Mehta, H. Bayley, and C. Dekker, "Hybrid Pore Formation by Directed Insertion of α-Haemolysin into Solid-State Nanopores," *Nat. Nanotechnol.*, vol. 5, no. 12, pp. 874–877, 2010.

[24]   M. Firnkes, D. Pedone, J. Knezevic, M. Döblinger, and U. Rant, "Electrically Facilitated Translocations of Proteins through Silicon Nitride Nanopores: Conjoint and Competitive Action of Diffusion, Electrophoresis, and Electroosmosis," *Nano Lett.*, vol. 10, no. 6, pp. 2162–2167, 2010.

[25]   U. F. Keyser, B. N. Koeleman, S. van Dorp, D. Krapf, R. M. M. Smeets, S. G. Lemay, N. H. Dekker, and C. Dekker, "Direct Force Measurements on DNA in a Solid-State Nanopore," *Nat. Phys.*, vol. 2, no. 7, pp. 473–477, 2006.

[26]   S. van Dorp, U. F. Keyser, N. H. Dekker, C. Dekker, and S. G. Lemay, "Origin of the Electrophoretic Force on DNA in Solid-State Nanopores," *Nat. Phys.*, vol. 5, no. 5, pp. 347–351, 2009.

[27]   A. R. Hall, S. van Dorp, S. G. Lemay, and C. Dekker, "Electrophoretic Force on a Protein-Coated DNA Molecule in a Solid-State Nanopore," *Nano Lett.*, vol. 9, no. 12, pp. 4441–4445, Dec. 2009.

[28]   C. Plesa, N. van Loo, P. Ketterer, H. Dietz, and C. Dekker, "Velocity of DNA during Translocation through a Solid-State Nanopore," *Nano Lett.*, vol. 15, no. 1, pp. 732–737, 2015.

[29] R. M. M. Smeets, U. F. Keyser, D. Krapf, M.-Y. Wu, N. H. Dekker, and C. Dekker, "Salt Dependence of Ion Transport and DNA Translocation through Solid-State Nanopores," *Nano Lett.*, vol. 6, no. 1, pp. 89–95, 2006.

[30] D. Fologea, J. Uplinger, B. Thomas, D. S. McNabb, and J. Li, "Slowing DNA Translocation in a Solid-State Nanopore," *Nano Lett.*, vol. 5, no. 9, pp. 1734–1737, 2005.

[31] D. V. Verschueren, M. P. Jonsson, and C. Dekker, "Temperature Dependence of DNA Translocations through Solid-State Nanopores," *Nanotechnology*, vol. 26, no. 23, p. 234004, 2015.

[32] M. Wanunu, W. Morrison, Y. Rabin, A. Y. Grosberg, and A. Meller, "Electrostatic Focusing of Unlabelled DNA into Nanoscale Pores using a Salt Gradient," *Nat. Nanotechnol.*, vol. 5, no. 2, pp. 160–165, 2010.

[33] C. Plesa, N. van Loo, and C. Dekker, "DNA Nanopore Translocation in Glutamate Solutions," *Nanoscale*, vol. 7, no. 32, pp. 13605–13609, 2015.

[34] S. W. Kowalczyk, D. B. Wells, A. Aksimentiev, and C. Dekker, "Slowing Down DNA Translocation through a Nanopore in Lithium Chloride," *Nano Lett.*, vol. 12, no. 2, pp. 1038–1044, 2012.

[35] A. J. Storm, J. H. Chen, X. S. Ling, H. W. Zandbergen, and C. Dekker, "Fabrication of Solid-State Nanopores with Single-Nanometre Precision," *Nat. Mater.*, vol. 2, no. 8, pp. 537–540, 2003.

[36] B. Schiedt, L. Auvray, L. Bacri, G. Oukhaled, A. Madouri, E. Bourhis, G. Patriarche, J. Pelta, R. Jede, and J. Gierak, "Direct FIB Fabrication and Integration of 'Single Nanopore Devices' for the Manipulation of Macromolecules," *Microelectron. Eng.*, vol. 87, no. 5–8, pp. 1300–1303, 2010.

[37] H. Kwok, K. Briggs, and V. Tabard-Cossa, "Nanopore Fabrication by Controlled Dielectric Breakdown," *PLoS ONE*, vol. 9, no. 3, p. e92880, 2014.

[38] P. Sigmund, "Mechanisms and Theory of Physical Sputtering by Particle Impact," *Nucl. Instrum. Methods Phys. Res. Sect. B-Beam Interact. Mater. At.*, vol. 27, no. 1, pp. 1–20, 1987.

[39] J. Orloff, "High-Resolution Focused Ion-Beams," *Rev. Sci. Instrum.*, vol. 64, no. 5, pp. 1105–1130, 1993.

[40]   C. J. Lo, T. Aref, and A. Bezryadin, "Fabrication of Symmetric Sub-5 nm Nanopores using Focused Ion and Electron Beams," *Nanotechnology*, vol. 17, no. 13, pp. 3264–3267, 2006.

[41]   B. W. Ward, J. A. Notte, and N. P. Economou, "Helium Ion Microscope: A New Tool for Nanoscale Microscopy and Metrology," *J. Vac. Sci. Technol. B*, vol. 24, no. 6, pp. 2871–2874, 2006.

[42]   J. Yang, D. C. Ferranti, L. A. Stern, C. A. Sanford, J. Huang, Z. Ren, L.-C. Qin, and A. R. Hall, "Rapid and Precise Scanning Helium Ion Microscope Milling of Solid-State Nanopores for Biomolecule Detection," *Nanotechnology*, vol. 22, no. 28, p. 285310, 2011.

[43]   A. A. Tseng, "Recent Developments in Nanofabrication Using Focused Ion Beams," *Small*, vol. 1, no. 10, pp. 924–939, 2005.

[44]   F. Sawafta, A. T. Carlsen, and A. R. Hall, "Membrane Thickness Dependence of Nanopore Formation with a Focused Helium Ion Beam," *Sensors*, vol. 14, no. 5, pp. 8150–61, 2014.

[45]   R. dela Torre, J. Larkin, A. Singer, and A. Meller, "Fabrication and Characterization of Solid-State Nanopore Arrays for High-Throughput DNA Sequencing," *Nanotechnology*, vol. 23, no. 38, p. 385308, 2012.

[46]   L. Galla, A. Meyer, A. Spiering, A. Sischka, M. Mayer, A. R. Hall, P. Reimann, and D. Anselmetti, "Hydrodynamic Slip on DNA Observed by Optical Tweezers-Controlled Translocation Experiments with Solid-State and Lipid-Coated Nanopores," *Nano Lett.*, vol. 14, no. 7, pp. 4176-4182, 2014.

[47]   T. Lindahl, "Instability and Decay of the Primary Structure of DNA," *Nature*, vol. 362, no. 6422, pp. 709–715, 1993.

[48]   E. Cavalieri, M. Saeed, M. Zahid, D. Cassada, D. Snow, M. Miljkovic, and E. Rogan, "Mechanism of DNA Depurination by Carcinogens in Relation to Cancer Initiation," *IUBMB Life*, vol. 64, no. 2, pp. 169–179, 2012.

[49]   J. R. Alvarez-Dominguez, O. Amosova, and J. R. Fresco, "Self-Catalytic DNA Depurination Underlies Human β-Globin Gene Mutations at Codon 6 That Cause Anemias and Thalassemias," *J. Biol. Chem.*, vol. 288, no. 16, pp. 11581–11589, 2013.

[50]   M. M. Marshall, J. A. Ruzicka, E. W. Taylor, and A. R. Hall, "Detecting DNA Depurination with Solid-State Nanopores," *PLOS ONE*, vol. 9, no. 7, p. e101632, 2014.

[51]   M. M. Marshall, J. Ruzicka, O. K. Zahid, V. C. Henrich, E. W. Taylor, and A. R. Hall, "Nanopore Analysis of Single-Stranded Binding Protein Interactions with DNA," *Langmuir*, vol. 31, no. 15, pp. 4582–4588, 2015.

[52]   A. T. Carlsen, O. K. Zahid, J. A. Ruzicka, E. W. Taylor, and A. R. Hall, "Selective Detection and Quantification of Modified DNA with Solid-State Nanopores," *Nano Lett.*, vol. 14, no. 10, pp. 5488–5492, 2014.

[53]   M. Howarth, D. J. F. Chinnapen, K. Gerrow, P. C. Dorrestein, M. R. Grandy, N. L. Kelleher, A. El-Husseini, and A. Y. Ting, "A Monovalent Streptavidin with a Single Femtomolar Biotin Binding Site," *Nat. Methods*, vol. 3, no. 4, pp. 267–273, 2006.

[54]   M. Fairhead, D. Krndija, E. D. Lowe, and M. Howarth, "Plug-and-Play Pairing via Defined Divalent Streptavidins," *J. Mol. Biol.*, vol. 426, no. 1, pp. 199–214, 2014.

[55]   C. A. Merchant, K. Healy, M. Wanunu, V. Ray, N. Peterman, J. Bartel, M. D. Fischbein, K. Venta, Z. Luo, A. T. C. Johnson, and M. Drndić, "DNA Translocation through Graphene Nanopores," *Nano Lett.*, vol. 10, no. 8, pp. 2915–2921, 2010.

[56]   G. F. Schneider, S. W. Kowalczyk, V. E. Calado, G. Pandraud, H. W. Zandbergen, L. M. K. Vandersypen, and C. Dekker, "DNA Translocation through Graphene Nanopores," *Nano Lett.*, vol. 10, no. 8, pp. 3163–3167, 2010.

[57]   K. Liu, J. Feng, A. Kis, and A. Radenovic, "Atomically Thin Molybdenum Disulfide Nanopores with High Sensitivity for DNA Translocation," *ACS Nano*, vol. 8, no. 3, pp. 2504–2511, 2014.

[58]   S. Liu, B. Lu, Q. Zhao, J. Li, T. Gao, Y. Chen, Y. Zhang, Z. Liu, Z. Fan, F. Yang, L. You, and D. Yu, "Boron Nitride Nanopores: Highly Sensitive DNA Single-Molecule Detectors," *Adv. Mater.*, vol. 25, no. 33, pp. 4549–4554, 2013.

[59]   K. Venta, G. Shemer, M. Puster, J. A. Rodriguez-Manzo, A. Balan, J. K. Rosenstein, K. Shepard, and M. Drndić, "Differentiation of Short, Single-Stranded DNA Homopolymers in Solid-State Nanopores," *ACS Nano*, vol. 7, no. 5, pp. 4629–4636, 2013.

[60]   D. J. Niedzwiecki, C. J. Lanci, G. Shemer, P. S. Cheng, J. G. Saven, and M. Drndić, "Observing Changes in the Structure and Oligomerization State of a Helical Protein Dimer Using Solid-State Nanopores," *ACS Nano*, 2015.

[61]   M. M. Marshall, J. Yang, and A. R. Hall, "Direct and transmission milling of suspended Silicon Nitride membranes with a Focused Helium Ion beam," *Scanning*, vol. 34, no. 2, pp. 101–106, 2012.

[62]   D. Santamore, K. Edinger, J. Orloff, and J. Melngailis, "Focused Ion Beam Sputter Yield Change as a Function of Scan Speed," *J. Vac. Sci. Technol. B*, vol. 15, no. 6, pp. 2346–2349, 1997.

[63]   A. R. Hall, "In Situ Thickness Assessment During Ion Milling of a Free-Standing Membrane Using Transmission Helium Ion Microscopy," *Microsc. Microanal.*, vol. 19, no. 3, pp. 740–744, 2013.

[64]   J. E. Hall, "Access Resistance of a Small Circular Pore.," *J. Gen. Physiol.*, vol. 66, no. 4, pp. 531–532, Oct. 1975.

[65]   M. Wanunu, J. Sutin, B. McNally, A. Chow, and A. Meller, "DNA Translocation Governed by Interactions with Solid-State Nanopores," *Biophys. J.*, vol. 95, no. 10, pp. 4716–4725, 2008.

[66]   M. van den Hout, V. Krudde, X. J. A. Janssen, and N. H. Dekker, "Distinguishable Populations Report on the Interactions of Single DNA Molecules with Solid-State Nanopores," *Biophys. J.*, vol. 99, no. 11, pp. 3840–3848, 2010.

[67]   S. W. Kowalczyk and C. Dekker, "Salt and Voltage Dependence of the Conductance Blockade Induced by Translocation of DNA and RecA Filaments Through Solid-state Nanopores," In Nanopores for Bioanalytical Applications; Edel, J., Albrecht, T., Eds.; Royal Society of Chemistry: London, 2012.

[68]   S. W. Kowalczyk and C. Dekker, "Measurement of the Docking Time of a DNA Molecule onto a Solid-State Nanopore," *Nano Lett.*, vol. 12, no. 8, pp. 4159–4163, 2012.

[69]   A. T. Carlsen, O. K. Zahid, J. Ruzicka, E. W. Taylor, and A. R. Hall, "Interpreting the Conductance Blockades of DNA Translocations through Solid-State Nanopores," *ACS Nano*, vol. 8, no. 5, pp. 4754–4760, 2014.

[70]   J. Ma, Y. Qiu, Z. Yuan, Y. Zhang, J. Sha, L. Liu, L. Sun, Z. Ni, H. Yi, D. Li, and Y. Chen, "Detection of Short Single-Strand DNA Homopolymers with Ultrathin Si_3N_4 Nanopores," *Phys. Rev. E*, vol. 92, no. 2, p. 022719, 2015.

[71]   A. J. Heron, J. R. Thompson, B. Cronin, H. Bayley, and M. I. Wallace, "Simultaneous Measurement of Ionic Current and Fluorescence from Single Protein Pores," *J. Am. Chem. Soc.*, vol. 131, no. 5, pp. 1652–1653, 2009.

[72]   A. Ivankin, R. Y. Henley, J. Larkin, S. Carson, M. L. Toscano, and M. Wanunu, "Label-Free Optical Detection of Biomolecular Translocation through Nanopore Arrays," *ACS Nano*, vol. 8, no. 10, pp. 10774–10781, 2014.

[73]   B. N. Anderson, O. N. Assad, T. Gilboa, A. H. Squires, D. Bar, and A. Meller, "Probing Solid-State Nanopores with Light for the Detection of Unlabeled Analytes," *ACS Nano*, vol. 8, no. 11, pp. 11836–11845, 2014.

[74]   D. Axelrod, N. L. Thompson, T. P. Burghardt, "Total Internal Reflection Fluorescent Microscopy", *J. Microsc.*, vol. 129, no. 1, pp. 19-28, 1983

[75]   R. Roy, S. Hohng, and T. Ha, "A Practical Guide to Single-Molecule FRET," *Nat. Methods*, vol. 5, no. 6, pp. 507–516, 2008.

[76]   T. Schmidt, M. Zhang, I. Sychugov, N. Roxhed, and J. Linnros, "Nanopore Arrays in a Silicon Membrane for Parallel Single-Molecule Detection: Fabrication," *Nanotechnology*, vol. 26, no. 31, p. 314001, 2015.

[77]   S. V. Deshpande, E. Gulari, S. W. Brown, and S. C. Rand, "Optical Properties of Silicon Nitride Films Deposited by Hot Filament Chemical Vapor Deposition," *J. Appl. Phys.*, vol. 77, no. 12, pp. 6534–6541, 1995.

[78]   B.-H. Kim, C.-H. Cho, T.-W. Kim, N.-M. Park, G. Y. Sung, and S.-J. Park, "Photoluminescence of Silicon Quantum Dots in Silicon Nitride Grown by NH_3 and SiH_4," *Appl. Phys. Lett.*, vol. 86, no. 9, p. 091908, 2005.

[79]   F. Sawafta, B. Clancy, A. T. Carlsen, M. Huber, and A. R. Hall, "Solid-State Nanopores and Nanopore Arrays Optimized for Optical Detection," *Nanoscale*, vol. 6, no. 12, pp. 6991–6996, 2014.

[80]   O. N. Assad, N. Di Fiori, A. H. Squires, and A. Meller, "Two Color DNA Barcode Detection in Photoluminescence Suppressed Silicon Nitride Nanopores," *Nano Lett.*, vol. 15, no. 1, pp. 745–752, 2015.

[81]   P. R. Srinivas, B. S. Kramer, and S. Srivastava, "Trends in Biomarker Research For Cancer Detection," *Lancet Oncol.*, vol. 2, no. 11, pp. 698–704, 2001.

[82]   N. Coppieters, B. V. Dieriks, C. Lill, R. L. M. Faull, M. A. Curtis, and M. Dragunow, "Global Changes in DNA Methylation and Hydroxymethylation in Alzheimer's Disease Human Brain," *Neurobiol. Aging*, vol. 35, no. 6, pp. 1334–1344, 2014.

[83]   D. Branton, D. W. Deamer, A. Marziali, H. Bayley, S. A. Benner, T. Butler, M. Di Ventra, S. Garaj, A. Hibbs, X. Huang, S. B. Jovanovich, P. S. Krstic, S. Lindsay, X. S. Ling, C. H. Mastrangelo, A. Meller, J. S. Oliver, Y. V. Pershin, J. M. Ramsey, R. Riehn, G. V. Soni, V. Tabard-Cossa, M. Wanunu, M. Wiggin, and J. A. Schloss, "The Potential and Challenges of Nanopore Sequencing," *Nat. Biotechnol.*, vol. 26, no. 10, pp. 1146–1153, 2008.
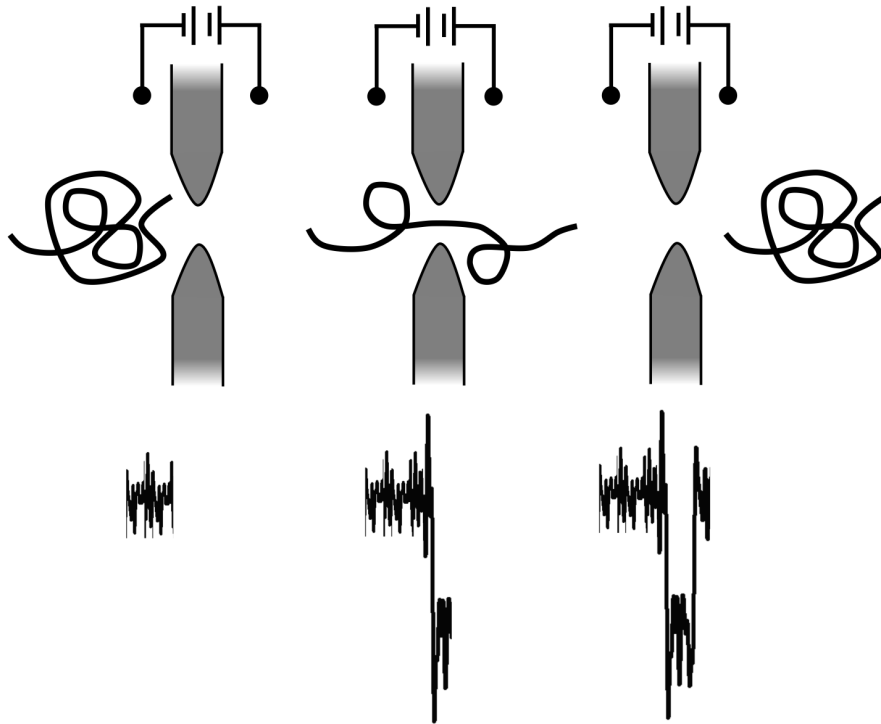
Figure 1. SS-Nanopore detection scheme Depiction of a biomolecule translocation with corresponding ionic current signal below: (a) baseline open-pore current; (b) threading of the molecule decreases ionic current; (c) current returns to baseline upon molecular passage. The total electrical signal is referred to as an event.
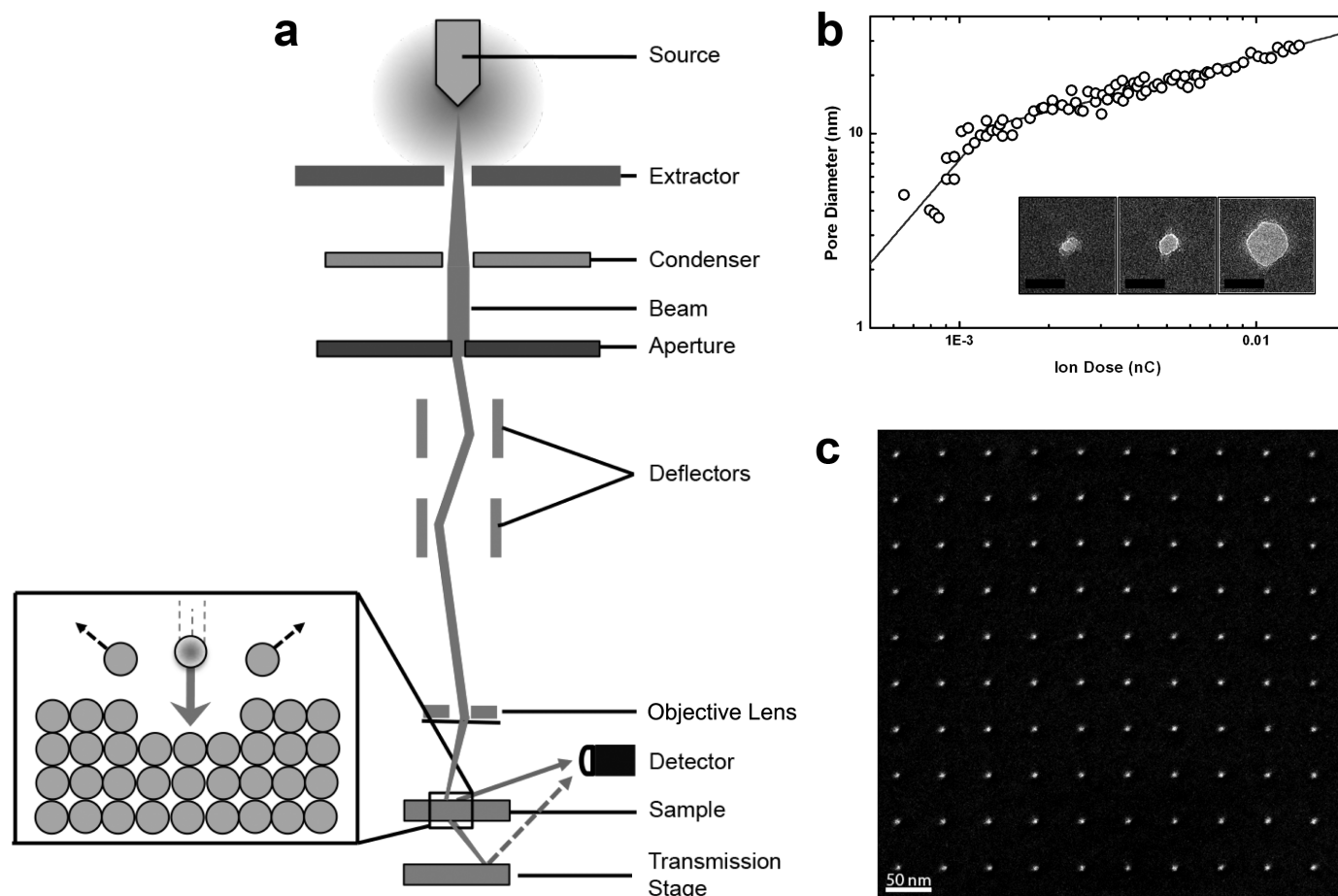
Figure 2. HIM Nanopore fabrication (a) Cross-sectional illustration of HIM components. Inset: schematic of nuclear interactions of the impinging ionic beam with sample. (b) Log–log plot of He+ dose versus resultant nanopore diameter showing a fast rate below ~10 nm and a slower one above. Solid lines are power law fits to the respective regions. Inset: TEM images of individual HIM nanopores with diameters (L-R) of 5, 10 and 20 nm. Scale bars are 20 nm. (c) STIM micrograph of a 10 × 10 array of 5 nm diameter nanopores.
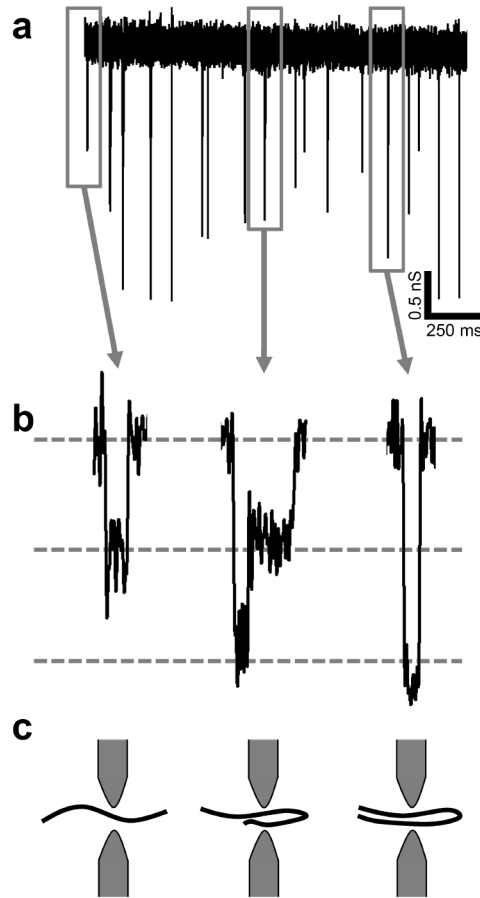
Figure 3. DNA translocation through HIM Nanopores (a) A typical measured conductance trace (150 mV applied voltage, low pass filtered at 5 kHz) showing downward spikes indicative of 48.8 kbp dsDNA translocations. (b) Examples of individual events from the conductance trace in (a), indicating the translocation of unfolded (left), partially folded (center) and folded (right) dsDNA. Dashed lines represent baseline and discrete conductance blockade levels. (c) Diagrammatic illustration of dsDNA conformation corresponding to each event in (b).
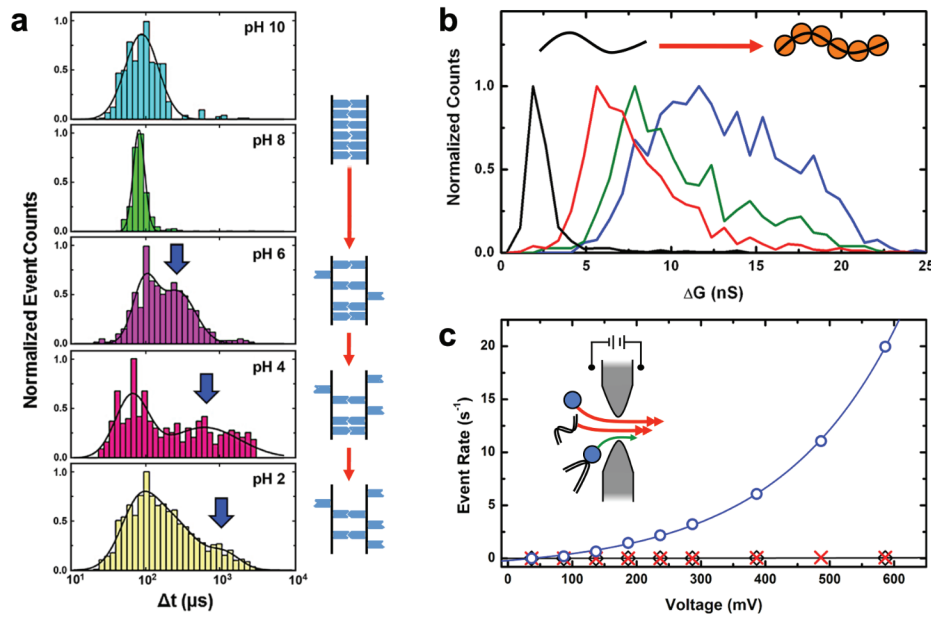
Figure 4. Applications of HIM Nanopores (a) Detecting DNA depurination[50]. Event duration histograms for 61 bp DNA translocation events from pH 10 (top) to pH 2 (bottom). Total numbers of events considered are n = 714 (pH 10), 662 (pH 8), 552 (pH 6), 423 (pH 4) and 1852 (pH 2). The black lines represent Gaussian fits to the data (pH 10 & 8: single peak; pH 6 & 4: two peaks; pH 2: three peaks). The prolonged translocation dwell times (blue arrows) indicate progressive DNA damage represented by the cartoon schematic next to the histograms. From Ref. 50. (b) Nucleoprotein complex analysis[51]. Mean conductance blockade (*ΔG*) histograms for ssDNA incubated with SSB in ratios of 1:0 (ssDNA alone, n = 551, black), 1:114 (n = 1048, red), 1:199 (n = 682, green), and 1:284 (n = 517, blue). The illustration (top) represents progressive complex formation as SSB concentration is increased. (c) DRNT detection of modified dsDNA[52]. Event rate vs. applied voltage for 150 bp dsDNA containing a single biotin (red crosses), MS (black diamonds) and dsDNA:MS (blue circles). DNA concentration was 1 μM and MS concentration was 2 μM. Solid lines are exponential fits to the data. Inset: Illustration of DRNT differentiation of dsDNA:MS complex (green arrow) from either constituent molecule.
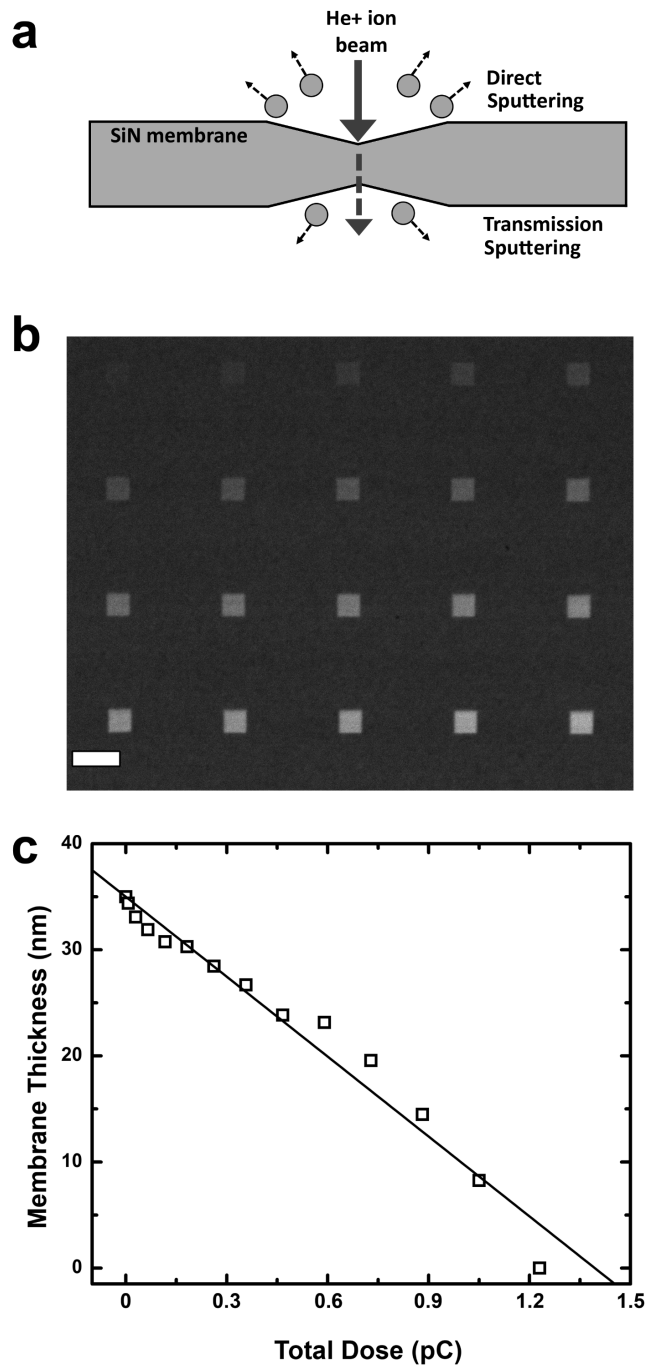
Figure 5. Manipulation of device thickness (a) Schematic representation of direct and transmission milling. Arrow indicates incident He+ ion beam and milling direction. (b) STIM micrograph of an array of 100 nm squares milled in a SiN membrane. Scale bar is 200 nm. (c) Relationship between total He+ ion dose and remaining thickness of a SiN membrane (initial thickness 35 nm), determined *in situ* by measuring relative STIM brightness of patterned regions compared to native membrane.
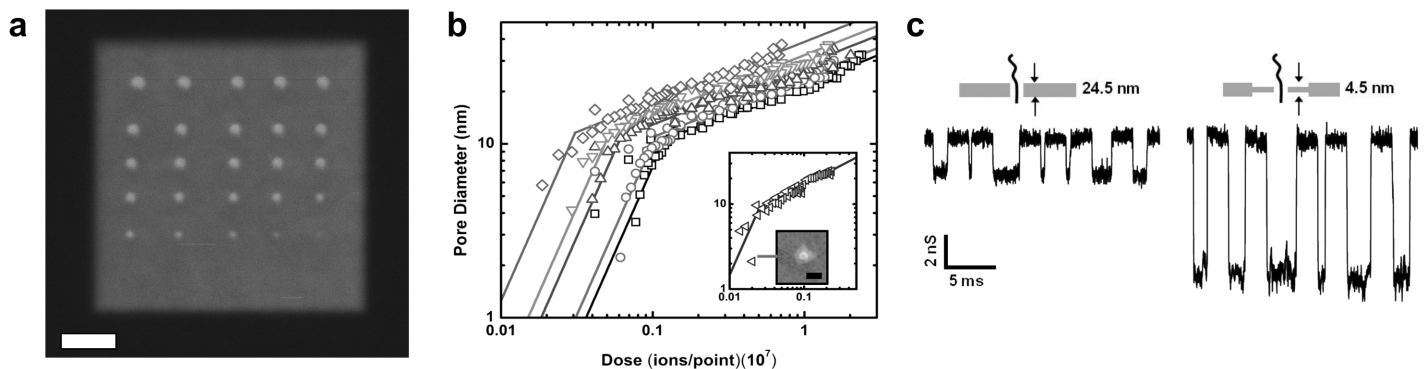
Figure 6. Fabrication of ultrathin nanopore devices (a) STIM micrograph of a nanopore array fabricated in a 500 nm^2 thinned region of the SiN membrane. Scale bar is 100 nm. (b) Log-log plot of ion dose vs. resulting pore diameter over a range of membrane thicknesses: (L-R) 4.5 nm (diamonds), 7.9 nm (downward facing triangles), 11.3 nm (upward facing triangles), 14.8 nm (circles), and 18.2 nm (squares). Each data set indicates a fast regime (left) and a slow regime (right) of pore growth with a transition in slope at a diameter of ~10 nm. Solid lines are power law fits to relevant sections of the data. Inset shows data for a 1.2 nm thick membrane, shown separately for clarity. Indicated data point is the smallest pore realized in that membrane (~2 nm diameter). (c) Concatenated event traces of dsDNA translocation measurements with two SS-nanopore devices: one 3.1 nm in diameter in a 24.5 ± 0.8 nm thick membrane (left) and one 3.2 nm in diameter in a 4.5 ± 0.6 nm thick membrane (right). All traces were low-pass filtered at 10 kHz. See Ref. 44.
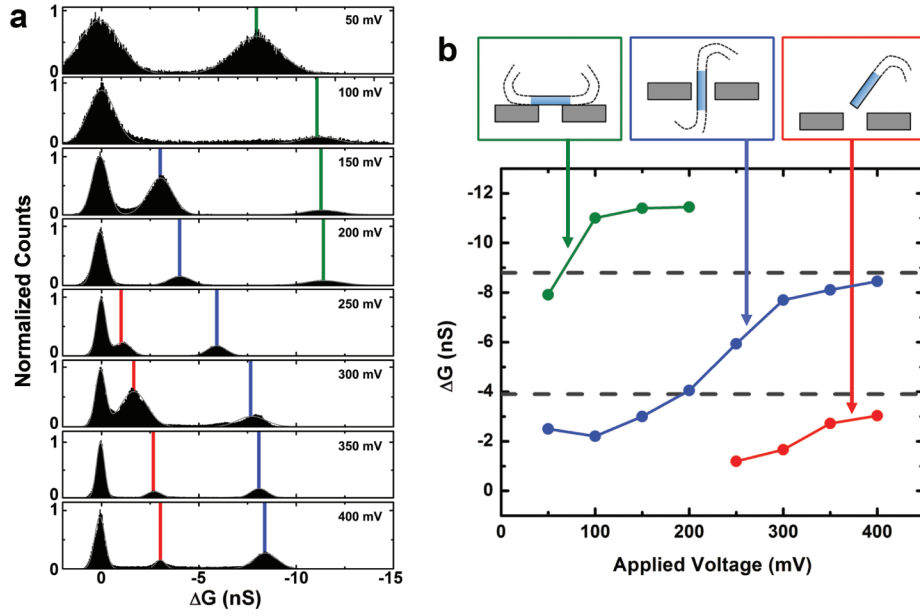
Figure 7. Application of HIM fabricated ultrathin nanopore devices (a) All-points histograms of (concatenated) conductance blockades from 50 to 400 mV (low-pass filtered at 10 kHz) for 3 kbp dsDNA using a 4.5 nm thick, 3.4 nm diameter SS-nanopore. In each panel, the left-most peak corresponds to the baseline (open-pore) conductance. Vertical lines indicate the center of the Gaussian fit (gray line) and indicate the evolution of individual conductance populations designated by color. (b) Average conductance change vs applied voltage. The dashed lines represent the calculated *ΔG* from geometric models[69] for the blue and red populations, respectively. Schematics (top) represent the DNA configuration proposed for each population. Colors match those in (a). See Ref. 69.
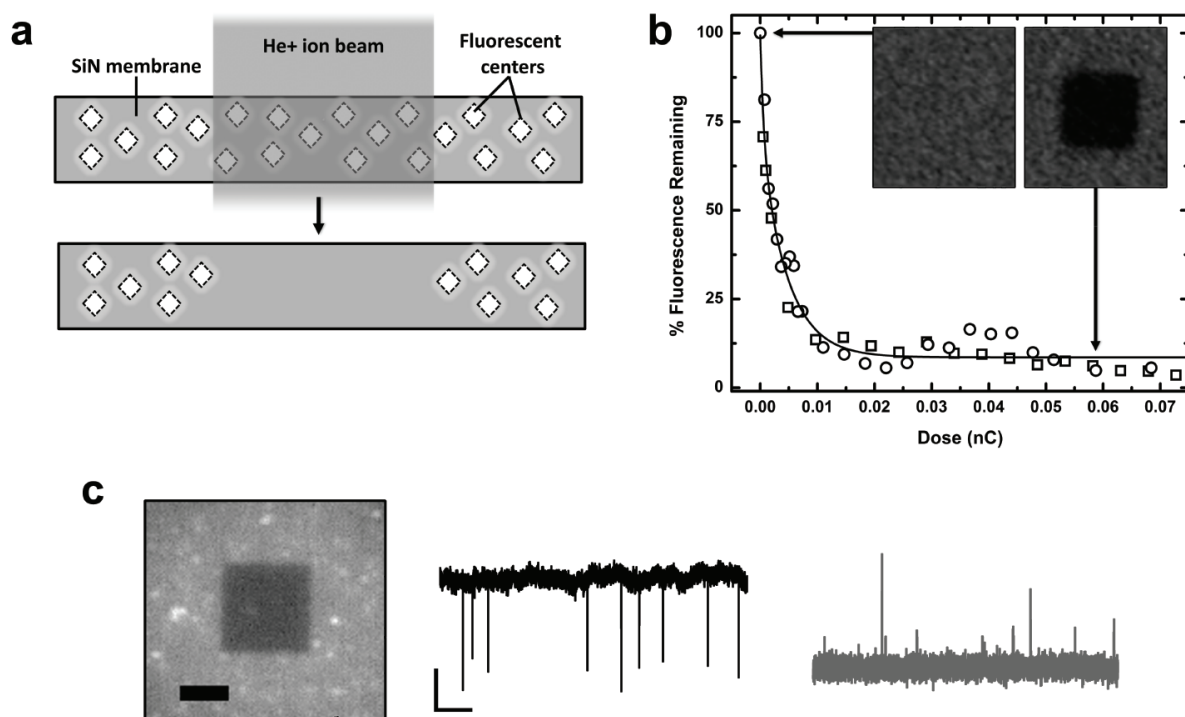
Figure 8. SiN membrane PL reduction by HIM (a) Schematic illustration of a native SiN membrane containing photoluminescent defects. Exposure to a low intensity He+ ion beam amorphizes these defects and thus reduces membrane PL. (b) Analysis of membrane fluorescence intensity in 500 nm^2 square patterns with varying He+ ion dose. Circles and squares are data from two separate chips and the solid line is an exponential fit to the data. Inset: fluorescence image of a native membrane (left) and nearly total PL suppression (right). Arrows indicate respective data points. (c) Optical image (left) of a He+ ion-bleached square containing a single SS-nanopore with diameter of 5 nm. Scale bar is 2 μm. Typical raw traces taken with the device, showing Cy3-labeled DNA translocation events using both conventional ionic conductance (center) and fluorescence intensity (right). Scale bar applies to both traces, with a horizontal scale of 2.5 s and a vertical scale of 0.5 nS (electrical) and 12.5 a.u. of gray scale (optical). See Ref. 79.
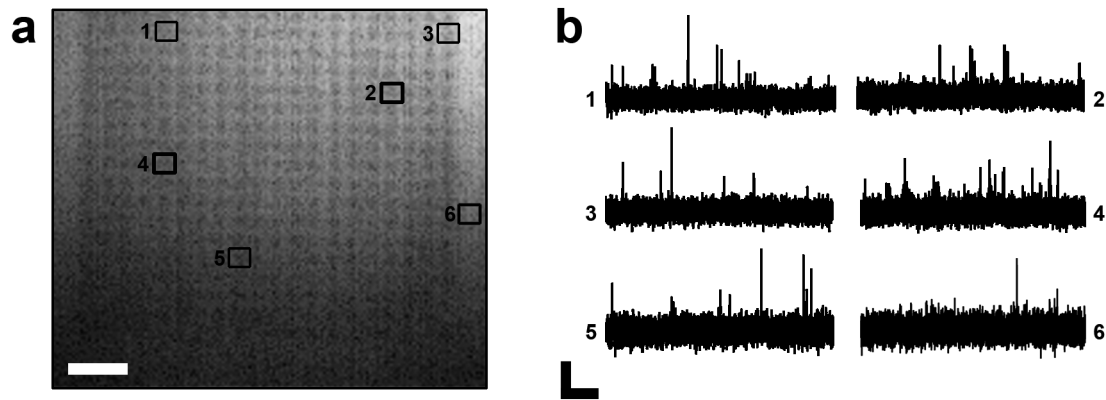
Figure 9. High-throughput optical detection of ssDNA translocations Fluorescence image of a 20 x 20 array of ~5 nm diameter SS-nanopores formed in a SiN membrane with locally-quenched background fluorescence. Image is an average of 100 video frames and contrast has been adjusted for clarity. Scale bar is 2.5 μm. (b) Raw fluorescence intensity traces measured simultaneously from video of Cy3-labeled ssDNA translocations through five typical nanopores within the array, each outlined with a square and numbered. Trace 6 is measured on a proximal region of the membrane with reduced-fluorescence but no pore. Scale bar is 0.5 s (horizontal) and 30 a.u. (vertical). See Ref. 79.
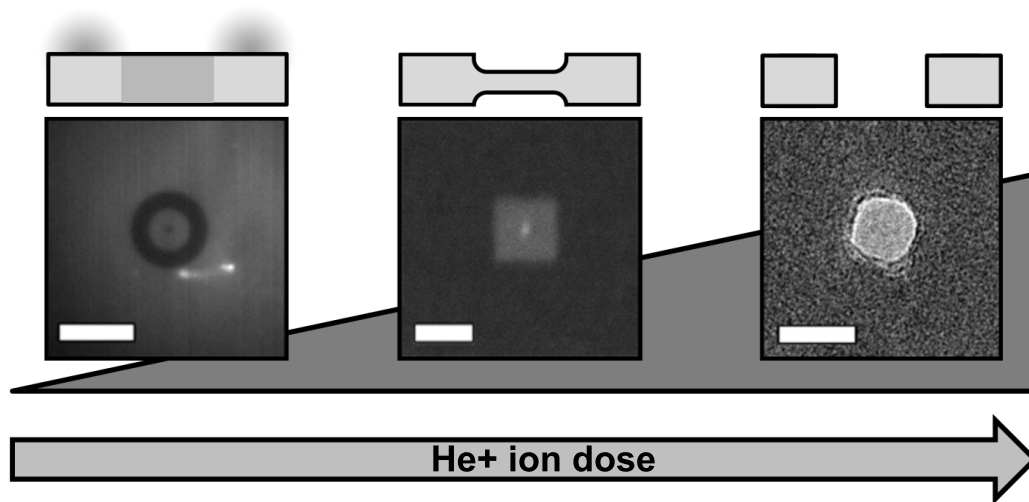
Figure 10. Manipulation of SS-nanopore device properties with He+ ions Varying He+ ion dose can be used to control a range of device properties. Images show: TIRF micrograph of a ring pattern (left) exposed to low He+ ion dose around a single pore, demonstrating PL reduction; STIM micrograph (center) of a nanopore (bright spot) fabricated in a square region of reduced thickness, demonstrating the effect of intermediate ion dose on membrane thickness; TEM image (right) of a ~20 nm diameter nanopore, demonstrating complete ablation of membrane material to form a pore. Scale bars are 4 μm, 100 nm, and 20 nm, respectively. Schematic above each image illustrates the affect of incident He+ ion dosage on membrane properties and dimensions.